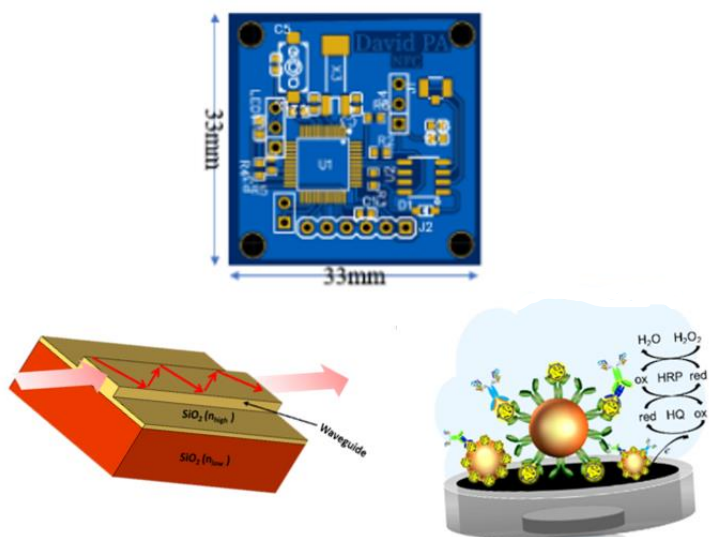


UM OLHAR SOBRE OS SENSORES NA PENÍNSULA IBÉRICA E AMÉRICA LATINA: ANO 2022

UNA MIRADA A LOS SENSORES EN LA PENÍNSULA IBÉRICA Y
AMÉRICA LATINA: AÑO 2022

A LOOK AT SENSORS IN THE IBERIAN PENINSULA AND LATIN
AMERICA: YEAR 2022



Coordenadoras
M. Teresa S. R. Gomes
Marta I. S. Veríssimo



universidade de aveiro
theoria potesis praxis

**UM OLHAR SOBRE OS SENSORES NA PENÍNSULA IBÉRICA E
AMÉRICA LATINA: ANO 2022**

UNA MIRADA A LOS SENSORES EN LA PENÍNSULA IBÉRICA Y AMÉRICA LATINA: AÑO 2022

A LOOK AT SENSORS IN THE IBERIAN PENINSULA AND LATIN AMERICA: YEAR 2022

12º Congresso Ibero-Americano de Sensores

Aveiro – PORTUGAL

M. Teresa S. R. Gomes e Marta I. S. Veríssimo

(coordenadoras)

FICHA TÉCNICA

Título:

Um olhar sobre os sensores na Península Ibérica e América Latina: Ano 2022

Coordenadoras:

M. Teresa S. R. Gomes, Marta I. S. Veríssimo

Revisores:

Carlos Domínguez-Horna | Carlos Silva Cárdenas | Cecilia Jiménez-Jorquera | Cyro Ketzer Saul | Enrique Ernesto Valdés Zaldívar | Fredy Segura-Quijano | Hesner Coto Fuentes | Idalia Ramos | Jahir Orozco Holguín | João A. B. P. Oliveira | José Antonio Plaza | José Antonio Rodríguez | Julián Alonso-Chamarro | Manel del Valle | Manuela Vieira | Marcelo Bariatto | María Gabriela Calle | M. Teresa S. R. Gomes | Mariano Aceves | Mário Ricardo Gongora-Rubio | Marta I. S. Veríssimo | Olimpia Arias de Fuentes | Salvador Alegret

Design e paginação:

Marta I. S. Veríssimo

Editora:

UA Editora

Universidade de Aveiro

Serviços de Documentação, Informação Documental e Museologia

1ª edição – Julho 2022

e-ISBN:

978-972-789-792-6

DOI:

<https://doi.org/10.48528/h76t-t092>

Os conteúdos apresentados são da exclusiva responsabilidade dos respetivos autores. © Autores. Esta obra encontra-se sob a Licença Internacional Creative Commons Atribuição 4.0.

Agradecemos o apoio financeiro ao CESAM através da FCT/MCTES (UIDP/50017/2020 + UIDB/50017/2020 + LA/P/0094/2020UIDP), através de fundos nacionais.

ÍNDICE | ÍNDICE | INDEX

| | |
|--|----|
| Prefácio | 9 |
| Prefacio | 11 |
| Preface | 13 |
| CONVIDADOS INVITADOS INVITED | 15 |
| <i>Implantable neural probes</i> | 17 |
| <i>Recent developments in nanostructured electrochemical sensors and biosensor platforms and applications</i> | 21 |
| <i>Chemical sensors and “real” analytical chemistry</i> | 25 |
| SENSORES ELECTROQUÍMICOS SENSORES ELECTROQUÍMICOS ELECTROCHEMICAL SENSORS | 29 |
| <i>Electrochemical nano-immunosensor based on cerium oxide-doped PEDOT nanocomposite for the detection of anti-p53 autoantibodies</i> | 31 |
| <i>Sensing ferrocene derivatives using a modified glassy carbon electrode with a PEDOT/carbon microspheres thin-film</i> | 34 |
| <i>Modified ISFETs with silk fibroin membrane for pH measurements in biological matrices</i> ... | 38 |
| <i>Lignosulfonate-based polyurethanes doped with carbon nanotubes towards sensor applications</i> | 43 |
| <i>Microelectrode sensors for corrosion studies</i> | 48 |
| <i>Optimization of an electrochemical phagomagnetic assay based on signal amplification of β-GLU-Cu₃(PO₄)₂ hybrid nanoflowers for selective quantification of live <i>Listeria monocytogenes</i></i> | 53 |
| <i>Two potentiometric microsensors for Cu²⁺ determination in corrosion processes</i> | 58 |
| <i>Dissolved oxygen biosensing using electrochemical electrodes and solid electrolyte polymer</i> | 65 |
| <i>Inkjet-printed electrode modified with magnetite particles and carbon nanotubes for the non-enzymatic amperometric determination of hydrogen peroxide</i> | 70 |
| <i>Novel ISE’s membranes formulation solvent and polymeric matrix free</i> | 74 |

SENSORES ÓTICOS E FOTOACÚSTICOS | SENSORES ÓPTICOS Y FOTOACÚSTICOS
| OPTICAL AND PHOTOACOUSTIC SENSORS 81

Biosensor based on polymer optical fiber and gold nanoparticle for rapid detection of Escherichia coli..... 82

Colorimetric based test-strips with virus-like particles as a recognition layer for SARS-CoV-2 virus..... 86

Single and cascaded long period fiber grating coated with a polydimethylsiloxane sensing film for acetone detection..... 91

Fe₃O₄-coated plastic optical fiber for H₂S sensing 96

Proposition of a photoacoustic based sensor for microplastic identification in marine environment..... 102

Oxygen sensor for oceanographic applications 107

Towards a NO_x microanalyser: miniaturized nitric oxide (NO) chemiluminescence analyzer prototype, for automotive industry applications..... 112

BIOSENSORES E APLICAÇÃO À ANÁLISE DE ALIMENTOS | BIODIAGNÓSTICOS Y APLICACIONES AL ANÁLISIS DE ALIMENTOS | BIODIAGNOSTICS AND APPLICATION TO FOOD ANALYSIS 117

Colorimetric pyranoflavylum-containing sensor films for food spoilage monitoring 118

Determinação cinética de histamina usando uma sonda ratiométrica fotoluminescente combinando pontos quânticos de carbono e pontos quânticos ternários..... 122

Development of an electrochemical aptasensor for the detection of a banned antimicrobial in milk..... 127

Disposable molecularly imprinted electrochemical sensor containing reduced graphene oxide and nickel nanoparticles for determination of p-coumaric acid in fruit peels 132

NOVOS MATERIAIS | NUEVOS MATERIALES | NEW MATERIALS 137

Laser-induced graphene on polyimide and paper substrates for low-cost and flexible electrochemical biosensors 138

UV photodetector based on reduced graphene oxide and n-type Si heterojunction..... 142

Host-guest sensing system based on sulfonatocalixarene and pyranoflavylum dye for biogenic amine sensing during food spoilage 148

Photosensitive nanopolymersomes as electroactive species carriers: towards the development of biosensors..... 151

Natural nanostructured materials as tuneable photonic sensing platforms..... 155

| | |
|--|-------------------|
| <i>Colorimetric assays for cardiovascular biomarkers detection using gold nanoparticles.....</i> | <i>159</i> |
| <i>A flow injection setup to determine oxytetracycline with a piezoelectric quartz crystal.....</i> | <i>164</i> |
| <i>Simultaneous voltammetric determination of acetaminophen, ascorbic acid and uric acid by use of integrated array of sensors modified with mesoporous carbon and metallic nanoparticles and electronic tongue principles</i> | <i>169</i> |
| <i>Modification of natural photonic crystals by tailoring of the refractive index contrast</i> | <i>174</i> |
| <i>Synthesis of microparticles of Cu₂ZnSnS₄ by hydrothermal method and its application as Congo Red photocatalyst</i> | <i>178</i> |
| <i>Characterization of Al₂O₃ and SiO₂ ultra-thin films deposited by ALD for microfabricated rubidium vapor cells</i> | <i>181</i> |
| <i>Structural and optical properties of sprayed undoped ZnO thin films suitable for resistive gas sensors</i> | <i>185</i> |
| <i>SRO/nitride-based electrophotonics for sensing applications</i> | <i>190</i> |
| DESENHO E TECNOLOGIA DE SENSORES E MEMS DISEÑO Y TECNOLOGÍA DE SENSORES Y MEMS DESIGN AND TECHNOLOGY OF SENSORS AND MEMS | 195 |
| <i>CoNi and Ni-based barcodes toxicity for tagging and magnetic manipulation of HeLa cells</i> | <i>196</i> |
| <i>Photonic planar taper waveguide</i> | <i>201</i> |
| <i>Sistema electrónico para medición de calidad de sustancias: diseño e implementación</i> | <i>209</i> |
| <i>Projeto de encapsulamento de sensores inerciais usando tecnologia LTCC.....</i> | <i>214</i> |
| <i>MEMS-based fabrication of an atomic vapor cell for brain magnetic field measurement</i> | <i>218</i> |
| <i>MEMS rubidium vapor cell for optically pumped magnetometers</i> | <i>223</i> |
| <i>MEMS-based waveguide SiO₂ fabricated by RIE process for optical sensing.....</i> | <i>227</i> |
| <i>Rubidium vapor cells fabricated by additive manufacturing</i> | <i>231</i> |
| CONDICIONAMENTO DE SINAL E INSTRUMENTAÇÃO ACONDICIONAMIENTO DE SEÑAL Y INSTRUMENTACIÓN SIGNAL CONDITIONING AND INSTRUMENTATION | 237 |
| <i>Inexpensive corn starch based supercapacitor for signal conditioning and detection</i> | <i>238</i> |
| <i>Feature extraction acceleration by the prediction of the steady state response for solid state gas sensors.....</i> | <i>242</i> |
| <i>Integración de redes neuronales con sistemas analíticos integrados para la cuantificación de metales pesados en solución acuosa.....</i> | <i>247</i> |

| | |
|--|-----|
| <i>Multi-photon microscopy setup for integration in colonoscopes: an overview</i> | 252 |
| <i>Simulación de la instrumentación electrónica asociada al isfet mediante el circuito integrado CD-4007</i> | 257 |
| MICROSSISTEMAS ANALÍTICOS INTEGRADOS E LAB-ON-A-CHIP MICROSISTEMAS ANALÍTICOS INTEGRADOS Y LAB-ON-A-CHIP ANALYTICAL INTEGRATED MICROSYSTEMS AND LAB-ON-A-CHIP | 263 |
| <i>Microreactors in protein pegylation: towards higher yields and specificity</i> | 264 |
| <i>Functionalization of a fully integrated electrophotonic silicon circuit for sensing biomolecules</i> | 270 |
| <i>Microanalizadores automáticos modulares para la monitorización de metales pesados en procesos hidrometalúrgicos</i> | 274 |
| <i>Optimización del sistema analítico integrado para el monitoreo de ión cobre en efluentes de una mina</i> | 279 |
| <i>Development of a microswitch made in LTCC-PDMS technology applicable to micro total analysis systems</i> | 284 |
| <i>Integração e automatização do funcionamento e do processo de aquisição de dados leitura de um sistema de sensores numa bancada de calibração de medidores de vazão de líquidos ..</i> | 289 |
| SENSORES INTELIGENTES E REDES SEM FIOS SENSORES INTELIGENTES Y REDES INALÁMBRICAS SMART SENSORS AND WIRELESS NETWORKS | 295 |
| <i>Architecture of a bi-directional VLC system for navigation and message transmission</i> | 296 |
| <i>Intelligent split intersections using cooperative vehicle visibility communication</i> | 301 |
| <i>A visible light communication system to support indoor guidance</i> | 307 |
| <i>Wireless sensor network system for landslide monitoring</i> | 313 |
| SENSORES DE ONDAS ACÚSTICAS SENSORES DE ONDAS ACÚSTICAS ACOUSTIC WAVE SENSORS | 319 |
| <i>Automation of the drop-casting deposition method for polymeric sensing films over a quartz crystal microbalance</i> | 320 |
| <i>Development of a relative humidity pid control for the characterization of gas sensors based on quartz resonators</i> | 325 |
| <i>Response measurement acceleration of QCM-based gas sensors using the transient response</i> | 329 |

| | |
|---|------------|
| APLICAÇÕES AO MEIO AMBIENTE E AGRICULTURA. POUPANÇA DE ENERGIA APLICACIONES AL MEDIO AMBIENTE Y A LA AGRICULTURA. AHORRO DE ENERGÍA APPLICATIONS TO THE ENVIRONMENT AND AGRICULTURE. ENERGY SAVING | 333 |
| <i>Plastic-optical-fiber-based solar tracker development applied for ambiences illumination .</i> | <i>334</i> |
| <i>Aveiro steam city project: a good practice with urban air quality sensors network.....</i> | <i>339</i> |
| <i>Intercomparison between air quality microsensors and conventional monitoring data</i> | <i>344</i> |
| <i>Sistema para el monitoreo de la calidad del aire en la zona metropolitana de la laguna.....</i> | <i>348</i> |
| <i>Evaluation of in-soil nutrient probes in different types of soils</i> | <i>353</i> |
| <i>Inductive salinity sensor.....</i> | <i>358</i> |
| APLICAÇÕES À BIOMEDICINA E À SAÚDE APLICACIONES A LA BIOMEDICINA Y A LA SALUD APPLICATIONS TO BIOMEDICINE AND HEALTH | 363 |
| <i>Biosensing strategies for exosomes.....</i> | <i>364</i> |
| <i>Simultaneous quantitative analysis of several electrolytes in sweat samples using a flow system and potentiometric devices</i> | <i>369</i> |
| <i>Impedimetric and capacitive biosensing of β-1,4-galactosyltransferase-v colon cancer biomarker.....</i> | <i>374</i> |
| <i>Disposable biomedical devices for at-home monitoring of different metabolic diseases.....</i> | <i>379</i> |
| <i>Surface modification of gallium nanoparticles and their interaction with human serum albumin</i> | <i>383</i> |
| <i>Detection of defects on displays based on microscopic and optical coherence tomography examination.....</i> | <i>388</i> |
| <i>Cu₂O/CuO composite synthesis by thermal treatment of Cu₂O thin films and its application as a non-enzymatic glucose sensor.....</i> | <i>392</i> |
| <i>Gallium nanoparticles interaction with IAPP: can GaNPs inhibits oligomerization?</i> | <i>396</i> |
| ÍNDICE DE AUTORES ÍNDICE DE AUTORES AUTHORS' INDEX | 401 |

P20 |

MEMS RUBIDIUM VAPOR CELL FOR OPTICALLY PUMPED MAGNETOMETERS

J. N. Vieira^{*}, H. M. Pereira, E. M. F. Vieira^{*}, J. A. Rodrigues, M. J. Maciel, J. H. Correia

¹ CMEMS - UMinho, University of Minho, 4800-058, Guimarães, Portugal

² LABBELS - Associate Laboratory, Braga, Guimarães, Portugal

^{*}e-mail: a83520@alunos.uminho.pt; d8408@dei.uminho.pt

Introduction

Magnetoencephalography (MEG) is the technique that allows direct imaging of the human brain electrophysiology, through the measurement of the magnetic fields generated by the neuronal currents in the brain scalp [1,2]. MEG technology uses superconducting quantum interference devices (SQUIDs), which require a cryogenic cooling system, and, consequently, thermal isolation. The main disadvantage of the SQUIDs is the loss of the neuromagnetic field detection, as the distance between magnetic source and sensor increases. In very recent years, there has been a scientific effort in the development of alternatives to SQUIDs, eliminating the need for cryogenic cooling equipment [3,4]. Optically pumped magnetometers (OPM) based on vapor cells of alkali-metals have emerged as a promising alternative to SQUIDs [5]. The main benefit of OPMs compared to SQUIDs is the precision of measurement in very low magnetic fields, without the requirement of complex cryogenic equipment, which reduces the volume of the MEG system and the maintenance costs [1–3,6,7]. The vapor cells allow for precise measurement of the magnetic fields using optical spectroscopy: the spin of the atoms forms a collective moment that changes in the presence of an external magnetic field, resulting in the variation of the transmittance of the vapor cell containing the atoms of the alkali-metal [3]. One significant advantage of OPMs is the microfabrication possibility [3,8], which is addressed in this work. The two most used and commercially available alkali-metals vapor cells (cesium and rubidium) were firstly compared. As a result of this comparison, a miniaturized cell fabrication based on the generation of alkali-metal vapor inside a sealed MEMS structure is proposed.

Methods

In OPMs, the increase of the external magnetic field is translated into a decrease of the light transmitted by the pump beam through the alkali-metal vapor cell.

This phenomenon is more prominent if the direction of the magnetic field is perpendicular to the light beam emitted. To compare the most used alkali-metal vapor cells for low magnetic field applications, a convenient optical-magnetic setup was created. Two commercially available alkali-metal vapor cells, from Thorlabs, were acquired for this purpose: rubidium-87 (^{87}Rb) isotope [9] and cesium (Cs) [10]. According to the results of this study, a complete design of the vapor cell miniaturization is here addressed. The fabrication process is based on the conventional glass-silicon-glass sandwich structure. Three main chemical reactions are currently used for the production of Rb/Cs considering the MEMS cells application, and are summarized in **Table I**.

Table I: Summary of the main chemical reactions used for alkali-metals production. X is Rb or Cs.

| Chemical reaction | Temperature | Observations | Ref. |
|--|-------------|--|------|
| $\text{BaN}_6 + \text{XCl} \rightarrow \text{BaCl} + 3\text{N}_2 + \text{X}$ | 200 °C | Reversible reaction could be occurred which limits the sensitivity of the magnetometer. | [8] |
| $2\text{XN}_3 \rightarrow 2\text{X} + 3\text{N}_2$ | 450 °C | Azide decomposition through UV light. | [11] |
| $2\text{XCl} + \text{Ca} \rightarrow 2\text{X} + \text{CaCl}_2$ | 720 °C | Deformation of glass windows due to high temperature reaction. Granular Ca forms limits dispensing in MEMS cells. | [12] |

Considering the proposed reactions, the alkali-metal azide decomposition is the most promising method for our proposed MEMS cells. It presents itself as a cost-effective solution, without the need for complex technological equipment, and the UV activation simplifies the decomposition process. Moreover, the photodecomposition method is advantageous in the sense that the azide product form is more stable at room temperature than the metal form of the material.

Results

Figure 1 represents the transmittance of the commercially available ^{87}Rb and Cs vapor cells for D1 transitions, 795 nm and 895 nm, respectively. The results obtained follow a biphasic exponential decay, characterized by being the sum of two decay processes happening at the same time: an initial fast decay for weak magnetic fields and a slow decay for stronger magnetic fields. Therefore, these results show a higher sensitivity for Rb vapor cells, as a more significant drop in the light transmittance is observed as a function of the magnetic field increase. According to this analysis, the Rb alkali-metal vapor cell is more suitable to be incorporated in OPMs.

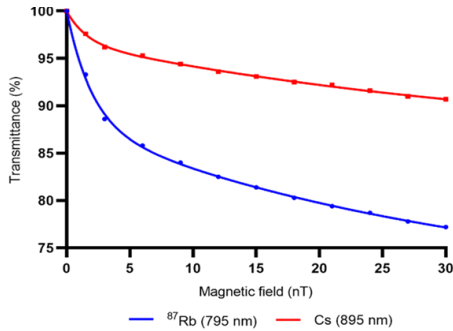


Figure 1 - Transmittance of light (%) as a function of magnetic field (nT), for the D1 transition of ^{87}Rb and Cs vapor cells, respectively.

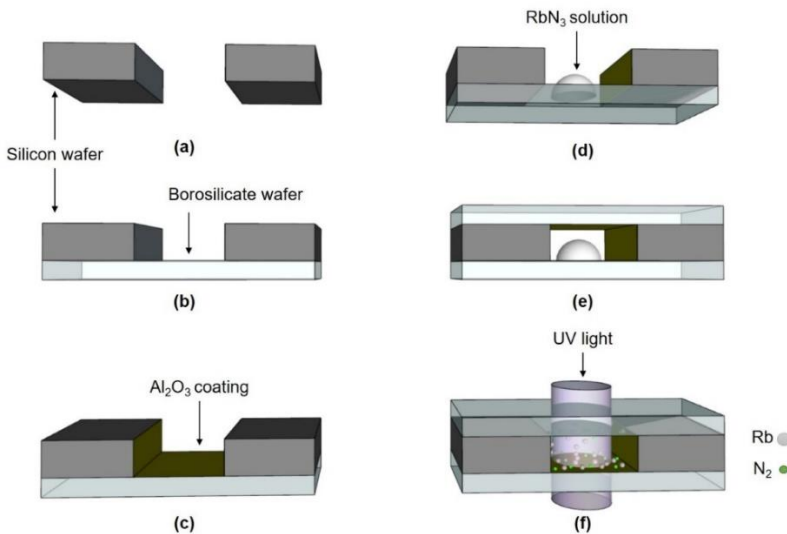


Figure 2 - (a-f) Process steps for obtaining the millimeter-level Rb vapor cell through decomposition of the alkali-metal azide by UV photolysis (not to scale).

One of the methods of MEMS cell fabrication includes the alkali compound decomposition induced by exposing encapsulated cells to UV radiation (see **Table I**). As a result, Rb and N_2 are obtained inside the cell. The steps of the proposed cell fabrication are shown in **Figure 2**, which include the preparation of silicon and borosilicate wafers; deep reactive ion etching (DRIE) of a silicon wafer, to obtain a millimeter-level cavity (Figure 2 (a)); anodic bonding between the first glass wafer and the bottom of the Si wafer (Figure 2 (b)); coating of all the cell walls with a Al_2O_3 thin layer to improve the vapor cell lifetime (Figure 2 (c)); micro-dispensing of the rubidium azide (RbN_3) aqueous solution into the millimeter-level cavity and dried at ambient atmosphere (Figure 2 (d)) and second anodic bonding of the top glass wafer, that will be performed at low temperature,

in order not to thermally decompose the alkali-metal azide compound ($< 300\text{ }^{\circ}\text{C}$), under controlled Ar atmosphere (Figure 2 (e)). In the last step, the metallic Rb and N_2 buffer gas will be created through UV irradiation of the RbN_3 aqueous solution, following the decomposition reaction: $2\text{RbN}_3 \rightarrow 2\text{Rb} + 3\text{N}_2$ - Figure 2 (f). For this purpose, a low-pressure lamp emitting at UV (peak wavelength of 254 nm) will be used. Long exposure is necessary to get a high yield decomposition of RbN_3 .

Conclusions

The transmittance results show that the ^{87}Rb alkali-metal vapor cell is more suitable to be incorporated in OPMs over the Cs cell. The fabrication of a millimeter-level alkali-metal vapor cells by using borosilicate and silicon wafers, through microfabrication technology is here proposed. This approach opens the perspective for massive production of OPMs and, therefore will contribute to the new generation of MEG based on OPMs, that will have high impact in diagnoses of some neurological diseases affecting the worldwide population, such as epilepsy and dementia.

References

1. T. H. Sander, J. Preusser, R. Mhaskar, J. Kitching, L. Trahms, and S. Knappe, *Biomed. Opt. Express* **3**, 981 (2012).
2. E. Boto, N. Holmes, J. Leggett, G. Roberts, V. Shah, S. S. Meyer, L. D. Muñoz, K. J. Mullinger, T. M. Tierney, S. Bestmann, G. R. Barnes, R. Bowtell, and M. J. Brookes, *Nature* **555**, 657 (2018).
3. C. Johnson, P. D. D. Schwindt, and M. Weisend, *Appl. Phys. Lett.* **97**, (2010).
4. M. Xie, J. F. Schneiderman, M. L. Chukharkin, A. Kalabukhov, B. Riaz, D. Lundqvist, S. Whitmarsh, M. Hamalainen, V. Jousmaki, R. Oostenveld, and D. Winkler, *IEEE Trans. Biomed. Eng.* **64**, 1270 (2017).
5. T. M. Tierney, N. Holmes, S. Mellor, J. D. López, G. Roberts, R. M. Hill, E. Boto, J. Leggett, V. Shah, M. J. Brookes, R. Bowtell, and G. R. Barnes, *Neuroimage* **199**, 598 (2019).
6. V. K. Shah and R. T. Wakai, *Phys. Med. Biol.* **58**, 8153 (2013).
7. V. Shah, S. Knappe, P. D. D. Schwindt, and J. Kitching, *Nat. Photonics* **1**, 649 (2007).
8. L.-A. Liew, S. Knappe, J. Moreland, H. Robinson, L. Hollberg, and J. Kitching, *Appl. Phys. Lett.* **84**, 2694 (2004).
9. Thorlabs - Rb, (2012).
10. Thorlabs - Cs, (2012).
11. L.-A. Liew, J. Moreland, and V. Gerginov, *Appl. Phys. Lett.* **90**, 114106 (2007).
12. W. Wei, J. Shang, W. Kuai, S. Qin, T. Wang, and J. Chen, in *2012 13th Int. Conf. Electron. Packag. Technol. High Density Packag.* (IEEE, 2012), pp. 1639–1641.

Acknowledgments

This work is supported by: Project MME reference 105399; CMEMS-UMinho Strategic Project UIDB/04436/2020 and UIDP/04436/2020; and Infrastructures Micro&NanoFabs@PT, NORTE-01-0145-FEDER-022090, Portugal 2020.

H. M. Pereira thanks FCT for the Ph.D. grant 2021.06647.BD.